Continuous welding of Cu–Ni dissimilar couple using CO_2 laser

G. Phanikumar[1], P. Dutta[2] and K. Chattopadhyay*[3]

The evolution of microstructure during continuous laser welding of dissimilar metals has been studied for a binary Cu–Ni couple. The effects of laser beam scan speed and laser power on the shape and size of the melt pool, the weldment–substrate interface, the composition profiles, and microstructures of the weldments have been investigated. It is shown that the melt pools exhibit a characteristic asymmetry in shape. The observed microstructure is characterised by the existence of compositional and microstructural variations leading to a banded appearance suggesting localised mixing. Distinct differences exist in the evolution of the microstructure in the copper and nickel sides of the weld pool. An attempt is made to explain some of the experimental observations using thermodynamic and thermal transport arguments.

Keywords: Microstructure, Continuous laser welding, Dissimilar metal couples, Cu–Ni couple, Laser beam scan speed, Laser power, Melt pool, Composition profiles

Introduction

Recent advances in manufacturing processes using lasers have led to increased use of advanced and dissimilar materials. The literature on the fusion weldments of dissimilar metallic joints is limited.[1–8] Considerable differences in the physical properties of the two metals lead to complexities in the weld pool shape, solidification microstructure, and segregation patterns. Conventional investigation in this field is usually limited to categorising the dissimilar welds according to the weld quality.[9,10] Efforts to gain insight into the complex physical processes and microstructural evolution that occur during dissimilar welding have been made by few research groups in recent years.[11–14]

During welding of dissimilar metals, the microstructural features that emerge as a result of differences in the physical properties of the two metals are potentially very different from the features observed in welding of similar metals/alloys. Solidification must occur from pure base metals into an alloy melt of different composition. A thermodynamic analysis is required to determine the conditions under which such a continuous growth is possible. Hence, from a scientific standpoint, analysis of a dissimilar metal joint offers a number of challenges.

The aim of the present work is to use Cu–Ni as a model dissimilar metal combination to characterise and explain the microstructural features typical of a dissimilar weld. Copper and nickel were selected as the dissimilar couple since they have different physical properties (*see* Table 1)[15] although the combination of pure metals has no direct application to the present authors' knowledge. The binary phase diagram indicates complete miscibility in solid and liquid states and thus the couple represents an ideal system for a detailed analysis. Laser welding was carried out at different scanning speeds, such that the welding mode changes from a conduction mode at high scan speed to a keyhole mode at low scan speed. Detailed microstructural analyses using optical microscopy, scanning electron microscopy, transmission electron microscopy, and quantitative composition analysis are presented. Thermodynamic and thermal transport arguments are

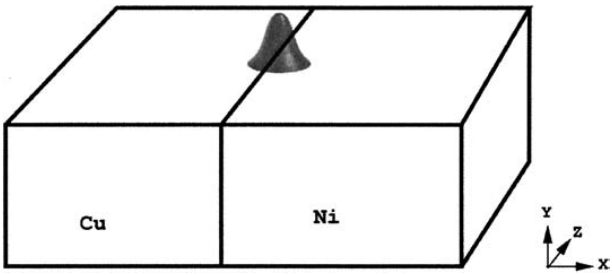

1 Schematic diagram of laser welding setup

Table 1 Physical properties of copper and nickel[15]

Property	Copper	Nickel
Melting point, °C	1083	1453
Thermal conductivity, W m^{-1} K^{-1}	399	88·5
Specific heat, J kg^{-1} K^{-1}	386	452
Density, kg m^{-3}	8900	7905
Thermal diffusivity, 10^{-5} m^2 s^{-1}	11·6	2·48
Latent heat, kJ mol^{-1}	13·02	17·16

[1]Department of Metallurgical and Materials Engineering, Indian Institute of Technology Madras, Chennai 600 036, India
[2]Department of Mechanical Engineering, Indian Institute of Science, Bangalore 560 012 India
[3]Department of Metallurgy, Indian Institute of Science, Bangalore 560 012, India
Work carried out in Department of Metallurgy, Indian Institute of Science

*Corresponding author, email gphani@iitm.ac.in

Published by Maney on behalf of the Institute
Received 28 November 2003; accepted 13 February 2004
DOI 10.1179/174329305X36043

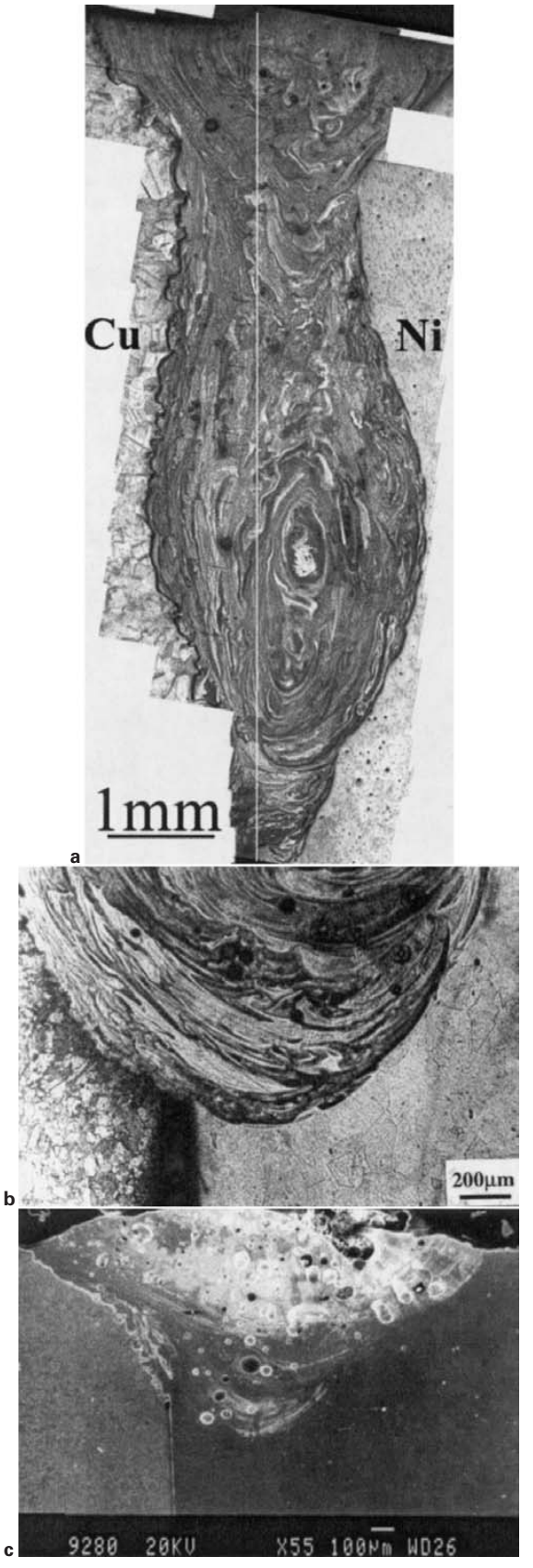

2 Cross-sectional view of Cu–Ni welds processed at *a* laser power of 5·5 kW and scan speed of 21 mm s^{-1} (optical), *b* 5·5 kW and 84 mm s^{-1} (optical), and *c* 4·5 kW and 4 mm s^{-1} (SEM)

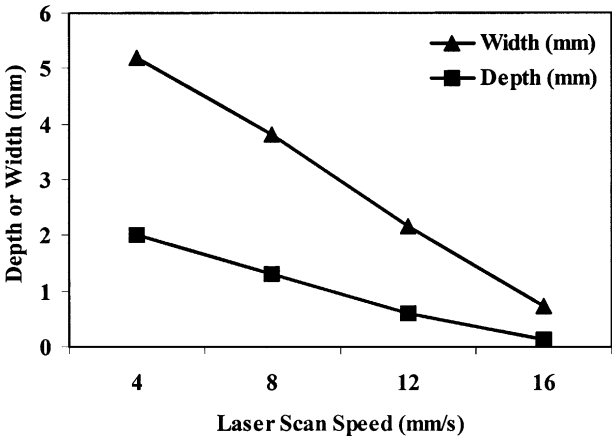

3 Variation of depth and width of weld pool as function of laser scan speed for laser power of 4·5 kW

used to explain the microstructural features observed. The study opens new challenges in the field of solidification of dissimilar alloy melts. To gain further insight into the physical processes, the authors have also performed a computational study, which is presented elsewhere.[16]

Experiments

A schematic diagram of the laser welding setup is shown in Fig. 1. The heat distribution is Gaussian and symmetric about the centreline on the top surface along the x and z axes. The two metals are received in the form of bars of dimensions $7 \times 7 \times 50$ mm and mounted in butt joint geometry on a computer numerical control table (accuracy within a few micrometres) with the parting line of the joint along the z axis. The joints are positioned with respect to the high power laser using a low power ruby laser. No coating is applied on the surface. The table is scanned along the z direction to form a continuous weld. Two sets of continuous welds are carried out with varying laser scan speed using commercially high purity copper and nickel. In the first set, laser scan speed is varied from 126 to 10·6 mm s^{-1} at a power of 5·5 kW. In the second set, laser scan speed is varied from 16 to 4 mm s^{-1} at a power of 4·5 kW. In the second set, the laser is slightly defocused to avoid formation of a keyhole. The welding conditions are summarised in Table 2. Weld samples are cut to provide

Table 2 Processing conditions used in continuous laser welding of Cu–Ni

Set	Laser	Beam diameter, mm	Gas shroud	Gas flowrate, $cm^3\ s^{-1}$	Laser power, kW	Scan speed, mm s^{-1}
1	Trumpf CW CO_2 laser, Zeiss optics	0·5	Ar–30 vol.-% He	~8	5·5	10·6 21 42 84 126
2	Rofin Sinar R10000 CW CO_2 laser	1	Ar	~120	4·5	4 8 12 16

CW continuous wave.

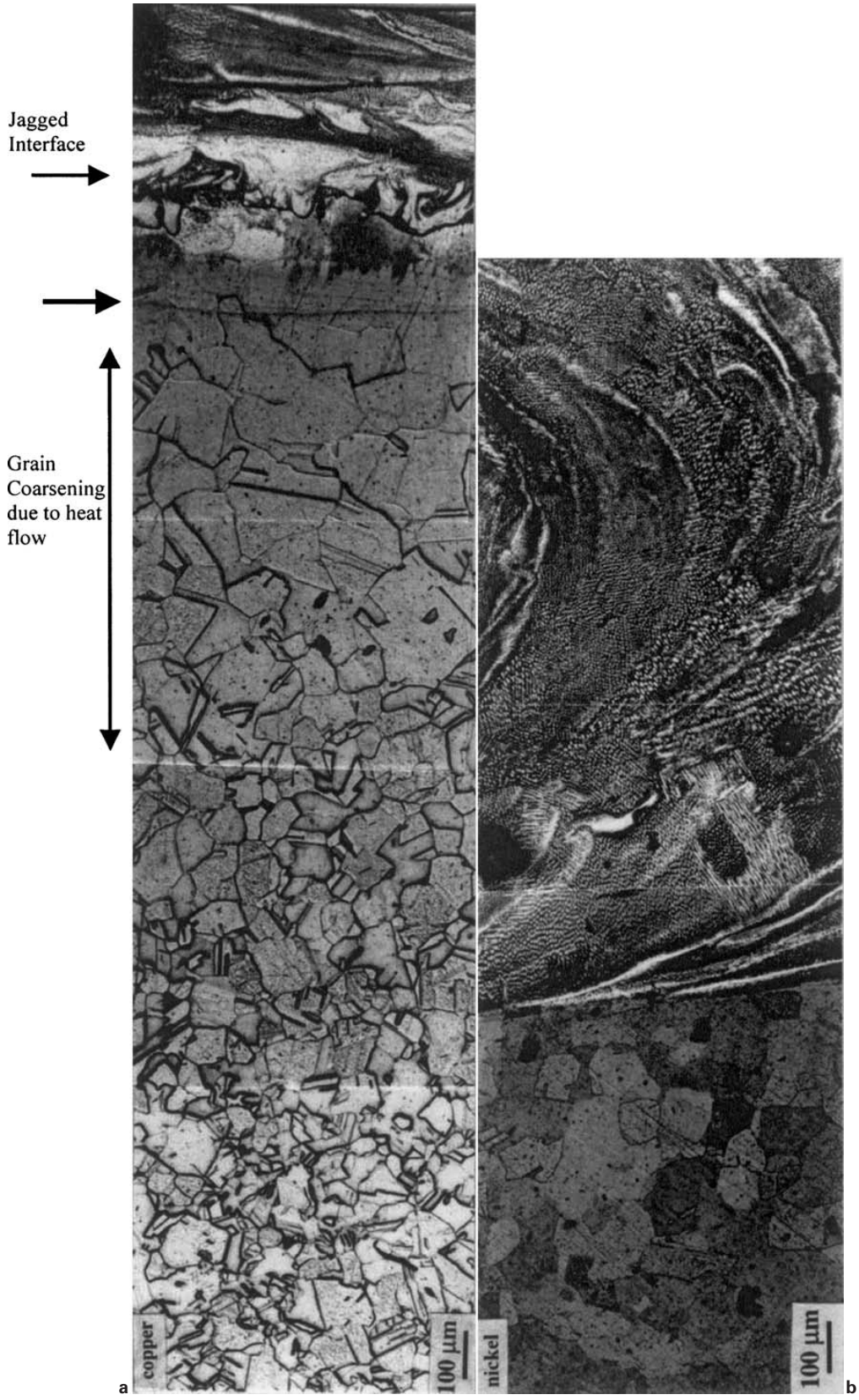

4 Top view showing microstructure of *a* copper side and *b* nickel side of weld at laser power of 5·5 kW and scan speed of 21 mm s^{-1} (optical)

transverse sections for characterisation. The microstructures were characterised via optical and scanning electron microscopy (Jeol model JSM 840). The composition analyses were carried out using an Oxford energy dispersive X-ray analysis facility attached to the SEM. Transmission electron microscopy of selected samples was performed using a Jeol 2000–FX II electron microscope operated at 200 kV. The samples for this purpose were prepared by ion milling using a Gatan dual ion beam mill.

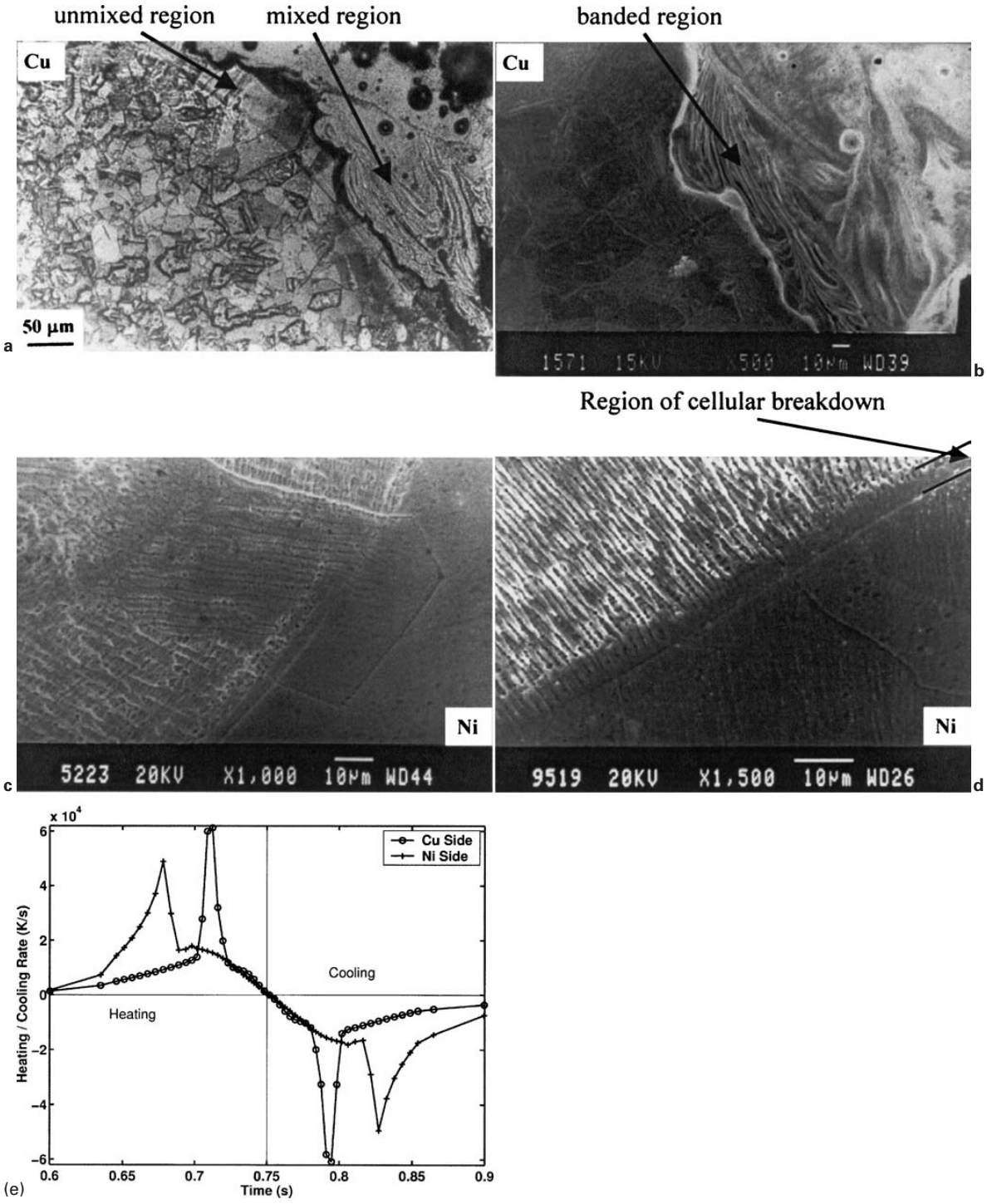

a copper side of interface, scan speed 4 mm s^{-1} (optical); *b* copper side, 12 mm s^{-1} (SEM); *c* nickel side, 4 mm s^{-1} (SEM); *d* nickel side, 12 mm s^{-1} (SEM); *e* heating (positive) and cooling rates (negative) experienced by two points at equal distance (0·2 mm) from centreline – results are extracted from previous work[16]

5 Weld interface microstructures in Cu–Ni weld produced at 4·5 kW and laser scan speeds of 4 and 12 mm s^{-1}

Microstructure analyses

The weld pool shapes at different scan speeds for the two laser powers (5·5 and 4·5 kW) are shown in Fig. 2. At low scan speeds, the weld processed with 5·5 kW laser power is deep and narrow indicating keyhole formation during welding (Fig. 2*a*). Weld pool depth in this instance is close to the sample thickness. As the laser scan speed is increased, the depth of penetration decreases. The melt pool is shallower, with an aspect ratio approaching a value of 2 for a scan speed of 84 mm s^{-1} (Fig. 2*b*). At lower power (4·5 kW) and low scan speeds, fully established keyhole formation could not be observed. However, the weld pool shape has a small dip at the bottom (Fig. 2*c*), indicating that there could have been some plasma formation during welding. The weld pool shapes at lower laser power and high scan speeds are shallower. The depth and width of the weld pool for various laser scan speeds, plotted in Fig. 3, exhibit the expected behaviour of decreasing in

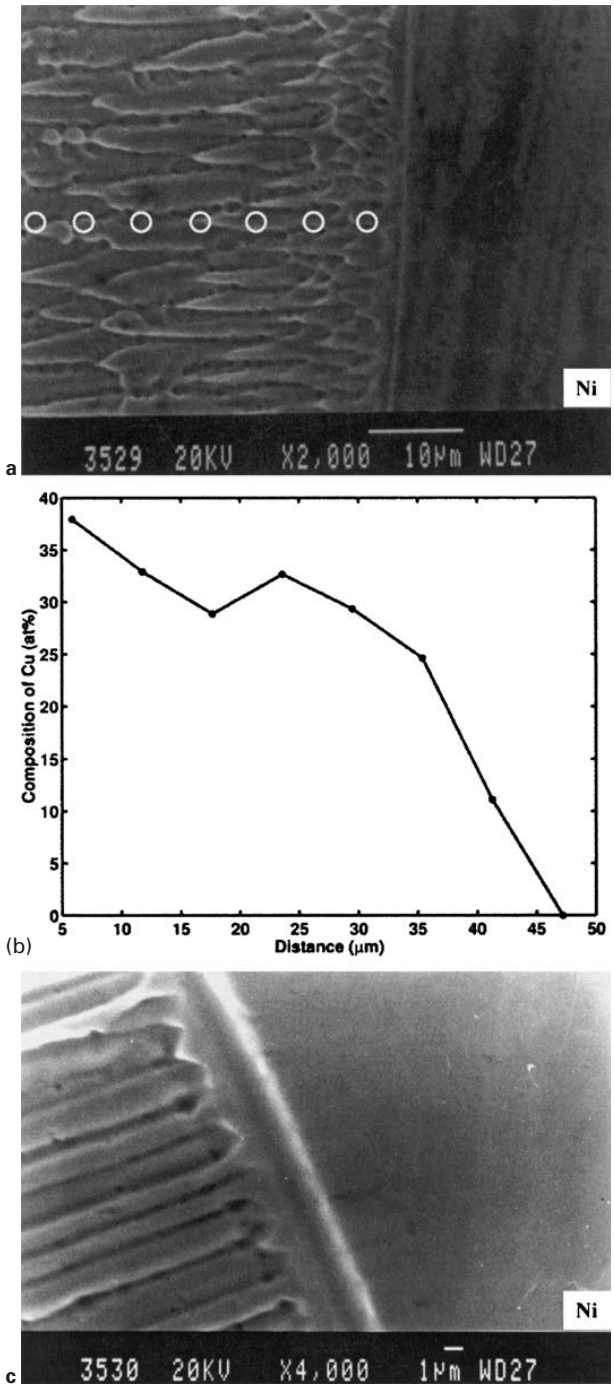

a microstructure – white circles show locations where EDS is taken (SEM); *b* variation of copper content; *c* high magnification, showing interface microstructure on nickel side of weld for same sample (SEM)

6 Composition variation from nickel interface into weld for laser power of 5·5 kW and scan speed of 42 mm s^{-1}

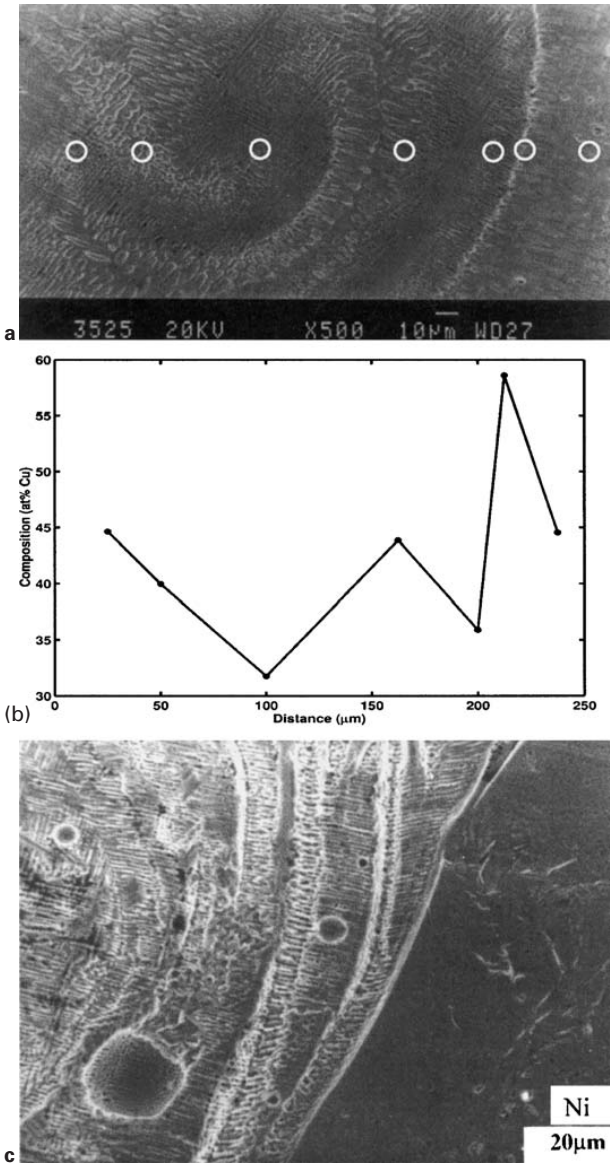

a microstructure at centre of weld (near eye) produced at 10·6 mm s^{-1} – white circles show locations where EDS is taken (SEM); *b* variation of copper content corresponding to *a*; *c* microstructure ahead of nickel interface near top of weld pool produced at 84 mm s^{-1} (SEM)

7 Microstructural banding and compositional variation in weld carried out at power of 5·5 kW and scan speeds of 10·6 and 84 mm s^{-1}

magnitude with increasing laser scan speed. An asymmetry in the pool shape with more melting of nickel is observed at all scan speeds and is more pronounced at higher scan speeds. At lower speeds a greater amount of copper melts, leading to a decrease in the asymmetry of the weld pool shape. Some porosity is also noted. The microstructure reveals segregation patterns and banding that are asymmetric in nature. At lower magnification they often have an appearance similar to the 'convective cell' (region of vortex formation in the liquid) like appearance observed in fluid flow.[12] At higher scan speeds, the 'eye' of the pattern lies on the nickel side (Fig. 2*b*) and at lower scan speeds, there is one 'eye' towards the top and one towards the bottom (Fig. 2*a*). Microstructural banding is less prominent at higher scan speeds.

The grain structure of the base metals showed no heat affected zone except for the welds processed at low scan speeds (10·6 and 21 mm s^{-1}) using a high laser power of 5·5 kW. A top view of the weld processed at a scan speed of 21 mm s^{-1} is shown in Fig. 4. The microstructure shows significant coarsening of copper grains but no such effect is noticeable on the nickel side. The starting grain size of copper is of the order of 100 μm, as can be seen in the parent metal away from the weld pool. The

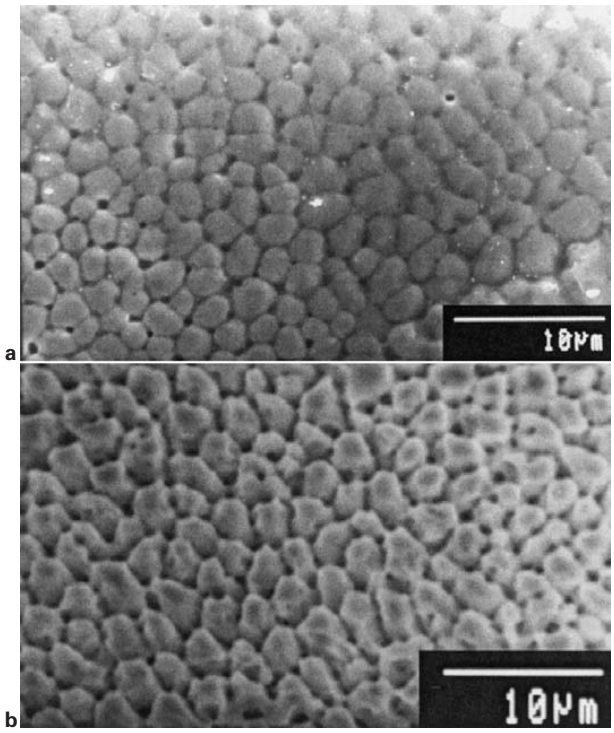

8 Cellular microstructures observed throughout weld regions for laser power of 4·5 kW and scan speed of 12 mm s^{-1} *a* near top of weld and *b* at centre of weld (SEM)

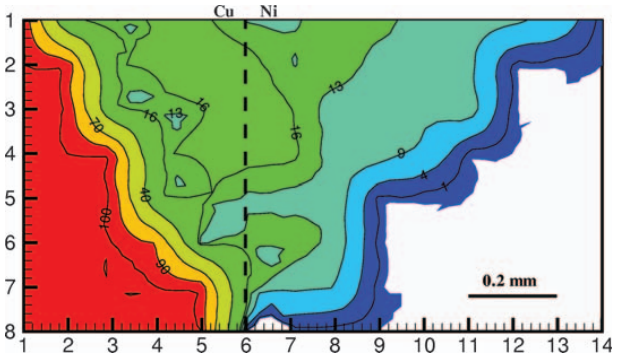

9 Composition map over whole of weld pool, with copper on left and nickel on right (dotted line indicates centreline of weld), for welds carried out at 4·5 kW and 8 mm s^{-1}: contour levels shown are in at.-%Cu

grains are considerably coarsened near the weld pool. The dark line revealing a slightly different etching effect at the weld interface, indicated by the arrow, shows the actual extent of fusion. No such effect is noticeable on the nickel side.

The microstructure mode of the weld interface can be clearly seen at higher magnification. On the copper side, the interface is rough with swirls of copper rich and nickel rich regions in an irregular pattern (Fig. 5*a* and *b*). The optical micrograph shown in Fig. 5*a* shows that on the copper side the extent of the fusion zone in the weld does not coincide with the region exhibiting significant mixing of copper and nickel. The interface between the mixed and unmixed regions is irregular, suggesting convective mixing at this interface. Figure 5*b* shows a SEM image of the same feature at higher magnification, revealing a banded structure in the mixed region.

In contrast, the nickel–weld interface is sharp and shows growth of the base metal into the weld (Fig. 5*c* and *d*). A distinct interface between the weld and the nickel region is distinguishable. In the microstructure, different grains of nickel can be seen growing into the weld with different cellular/dendritic pattern orientations. The composition variation along the normal to the cellular growth front from the base has been measured and is shown in Fig. 6*b*. The grains of nickel initially grow in a planar manner and as the copper content in the solidified region increases gradually, the microstructure changes to a cellular/dendritic mode. This is more readily discernible in the microstructure at a higher magnification shown in Fig. 6*c*. The scale of the microstructure also increases as growth proceeds into the weld, as can be seen in Fig. 6*a*.

Microstructural banding is observed throughout the weld, and in particular near the interface. Figure 7*a* shows a typical microstructural pattern observed at the centre of the weld. The bands are characterised by a change in composition as well as microstructural length scale. The cellular patterns are continuous across the bands. The shape of the bands closely follows the possible motion of the solidification front, as could also be seen in Fig. 7*c* (*see* also the bands in the top view in Fig. 4*b*). The microstructure is found to fluctuate from a fine scale to a coarse scale with concurrent compositional fluctuations away from the substrate. In an extreme case, the composition fluctuation near the nickel interface was found to vary from $\sim$4 to $\sim$20 at.-%Cu in two adjacent bands exhibiting cell free and cellular microstructure respectively. These bands were termed low velocity bands by Gremaud *et al.*[17] The microstructure throughout the weld exhibits a cellular/dendritic structure (Fig. 8). The cell spacing is found to be marginally smaller near the top of the weld region (Fig. 8*a*) compared with the interior (Fig. 8*b*) indicating a change in growth conditions from top to bottom.

To determine the composition distribution at a macroscopic scale across the weld, a large number of spot EDAX measurements were taken to cover the entire weld pool for two samples processed with laser powers and scan speeds of 5·5 kW/84 mm s^{-1} and 4·5 kW/8 mm s^{-1} respectively. The measured compositions are plotted in Fig. 9 using contours to reveal the distribution. As can be seen from Fig. 9, much of the weld region on the nickel side is well mixed with shallow composition gradients. On the copper side, the close spacing between the composition isolines indicates high compositional gradients and a lack of mixing.

A limited amount of TEM was carried out on the Cu–Ni welds. A typical microstructure from a region slightly towards the copper side of a weldment processed at 5·5 kW and 21 mm s^{-1} is shown in Fig. 10. The diffraction pattern (Fig. 10*c*) indicates formation of CuNi solid solution. The lattice spacing calculated from the electron diffraction patterns corresponds to a Cu–50 at.-%Ni alloy. In addition a faint reflection is observed, which can be attributed to internally oxidised Cu_2O (Fig. 10*d*). The presence of fine particles in the micrograph (Fig. 10*a* and *b*), as observed in some regions, confirms the above evidence. This suggests increased oxygen solubility during processing and

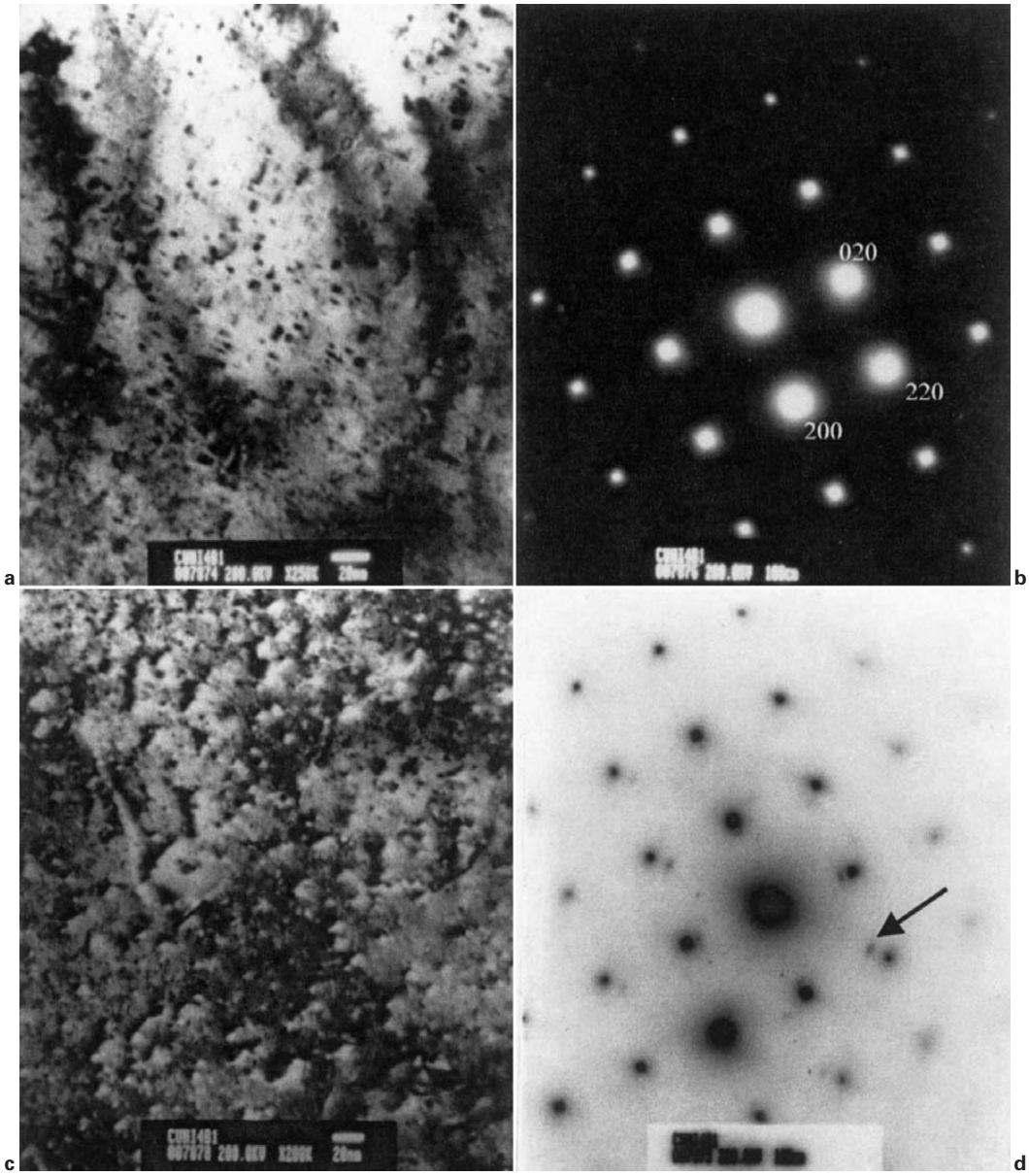

a bright field image taken in [001] zone; *b* dark field taken from (200) reflection; *c* diffraction pattern corresponding to *b*; *d* selected area diffraction pattern taken from region in *a* – arrow indicates extra spots

10 Transmission electron microscopy of Cu–Ni weld produced at 5·5 kW and 16 mm s^{-1}

subsequent oxide precipitation in the solid state. The presence of high strain contrast is also notable.

Discussion

Dissimilar welds of copper and nickel processed at two different laser powers using a range of scan speeds show several common features. The weld is asymmetric, with melting of more nickel than copper. Even though the melting point of copper is lower than that of nickel, the nickel melts first owing to its lower thermal diffusivity. The higher thermal conductivity of copper leads to less absorption of heat and thus a lesser extent of melting. The present authors have recently carried out a rigorous three-dimensional fluid flow model of the process, which is presented elsewhere.[16] The computational results are consistent with the present observations. At the macroscopic level, the overall composition in the weld pool is nearly uniform on the nickel side and shows a sharp variation on the copper side. Since the copper side of the weld spends considerably less time in the liquid state owing to higher heat transfer, mixing is not complete. The thermal cycles experienced by two points (one on the copper interface and the other on the nickel interface) at an equal distance of 0·2 mm from the centreline near the top of the sample are shown in Fig. 5*e*. The results are extracted from the computational work presented elsewhere[16] and correspond to welding conditions of 4·5 kW and 8 mm s^{-1}. The heating rates are plotted as positive, experienced as the laser approaches the point. The cooling rates are plotted as negative, experienced as the laser moves away from the point. As can be seen, the cooling rates are of the order of 10^4 K s^{-1} and are higher on the copper side. The higher heat flux through the copper substrate also leads to grain growth near the weld interface on the copper side. This is confirmed by experimental observations (Fig. 4*a*). The majority of the

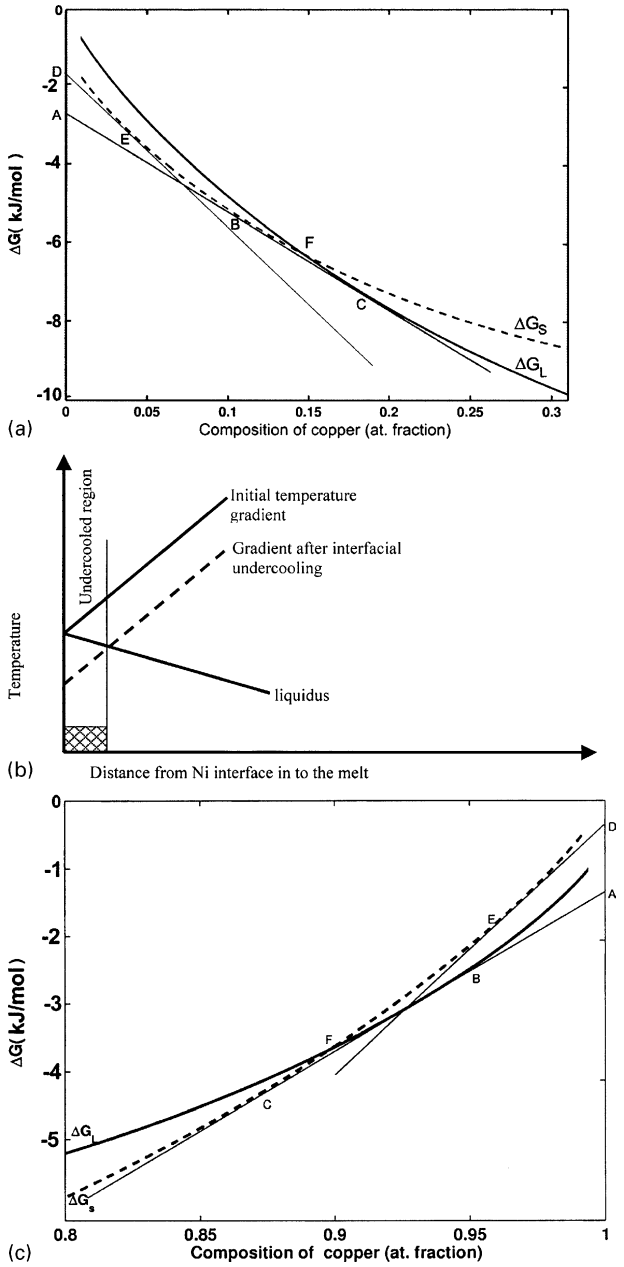

11 Thermodynamic analysis of solidification, showing *a* free energy versus composition plots for T=1400°C on nickel rich side, *b* schematic diagram demonstrating possibility of undercooled region (shaded) ahead of nickel interface, and *c* free energy versus composition plots for T=1140°C on copper rich side

observed microstructural bands in the weld pool, being normal to the solidification direction, suggest an oscillatory growth of solid into the melt. This type of growth develops as a result of a combination of an advancing solidification front driven by heat transfer through the base metal and the radial Marangoni convection outward from the centre of the laser bringing the hotter liquid in front of the solidification interface. The presence of such a growth mode was confirmed recently via a direct visualisation.[18]

The interface microstructures between the weldment and substrate are also asymmetric, with a continuous growth of nickel solid solution into the molten weld pool on the nickel side and ragged interface and distinct layering (and inhomogeneous mixing) on the copper side. In thermodynamic terms, the problem pertains to the growth of solid into a compositionally inhomogeneous melt. The transfer of atoms required for solidification is guided by the chemical potentials of the two species at the solidification interface. An analysis of the driving force required for the growth of a pure metal into an alloy pool can be made using the free energy versus composition curves. In the present case, the welding speeds are not high and justify the assumption of local equilibrium at the solid–liquid interface. Free energy data for the liquid and solid phases in the Cu–Ni binary system were obtained from the literature.[19]

Consider first whether the nickel interface which is in contact with the molten weld pool of composition C can grow into the melt (Fig. 11*a*). It is assumed that the composition of the nickel substrate at the interface marked E is slightly copper rich owing to diffusion. The common tangent construction of the free energy curve at the liquidus temperature indicates that the solid corresponding to the composition B will be at equilibrium with the liquid at this temperature. Considering the chemical potential of the nickel in the substrate at the interface (intercept of tangent at E with the vertical axis), it is evident that it is higher than that in the melt C. Thus, nickel atoms will tend to leave the interface and transfer to the melt. Thus the interface cannot grow and solidification can occur only by nucleation of solid in the melt. In the absence of nucleation the temperature of the weld pool substrate interface will decrease. This is shown in Fig. 11*b*. Conversely, copper atoms from the melt can move to the solid. Thus it is possible for nickel enrichment of the melt and copper enrichment of the solid to occur. These changes in the compositions will ultimately result in favourable conditions for the substrate to grow into the melt. However, as shown in Fig. 11*b* the growing solid will encounter, in addition to a composition gradient, a constitutionally supercooled regime during the process, leading to a cellular breakdown of the growth front and continuous change in cell spacing.

Consider the situation on the copper side. Figure 11*c* shows the free energy versus composition plot on the copper rich side for a temperature of 1140°C. An alloy liquid of composition Cu–7 at.-%Ni (marked C) is in equilibrium with a solid of higher nickel content (point B, Cu–13 at.-%Ni). The point F is the intersection of the solid and liquid free energy. Solids with nickel content less than that of F have higher free energy compared with liquids of the same composition at this temperature. Only solids with nickel content higher than that given by F can form from the melt. If the copper grains of the substrate were to grow continuously into the weld, their composition would have to increase beyond the value indicated by F by diffusion. Any intermediate composition (such as E) would melt back owing to its free energy being higher than that of the liquid of the same composition. Thus, it can be concluded that growth cannot occur from the copper substrate into the nickel rich melt. The solidification on the copper rich side occurs directly from the melt. The absence of any evidence of continuous growth from the copper side of the weld and the rough interface in the experiments corroborates this argument. Thus, the conventional arguments regarding epitaxial and continuous growth

of base metal into the weld, applicable for welds between similar alloys, cannot be extended to dissimilar welds as assumed by previous researchers.[20] It is becoming increasingly clear that the issues of nucleation and growth in the presence of a compositional gradient offer several interesting results.[21] A closer examination using thermodynamic aspects of the growth of solid into an inhomogeneous melt with quantitative estimates of driving forces could provide further insights.

Conclusions

Laser welding of copper and nickel performed at different scanning speeds shows a change of welding mode from conduction at high scan speed to keyhole at low scan speed. The weld pool shape and composition distribution were found to be asymmetric and the interface microstructure modes are found to be different on the two sides. Cellular microstructure with extensive banding was observed in the weldment at all welding speeds. The composition profile indicates that the nickel side is relatively well mixed. The nickel substrate can grow into the molten weld pool with a gradual increase in copper content. On the copper side, such a continuous growth of the substrate could not be observed. A thermodynamic argument was provided to explain this asymmetry. Examination via TEM showed that the weld pool is highly strained.

Acknowledgements

The authors thank Professor J. Mazumder and Professor B. L. Mordike for providing access to their experimental facilities and Dr R. Galun for his support in conducting part of the experiments.

References

1. J. Seretsky and E. R. Ryba: *Weld. J.*, July 1976, 208s–211s.
2. G. Metzger and R. Lison: *Weld. J.*, August 1976, 230s–240s.
3. C. Pan, R. Wang, J. Gui and Y. Shi: *J. Mater. Sci.*, 1990, **25**, 3281–3285.
4. Z. Sun and J. C. Ion: *J. Mater. Sci.*, 1995, **30**, 4205–4214.
5. B. Majumdar, R. Galun, A. Weisheit and B. L. Mordike: *J. Mater. Sci.*, 1997, **32**, 6191–6200.
6. S. Katayama, R. Usui and A. Matsunawa: Proc. 5th Int. Conf. on 'Trends in welding research', (ed. J. M. Vitek *et al.*), 467–472; 1998, Materials Park, OH, USA, ASM International.
7. G. Phanikumar, R. Pardeshi, K. Chattopadhyay, P. Dutta and J. Mazumder: Proc. 5th Int. Conf. on 'Trends in welding research', (ed. J. M. Vitek *et al.*), 461–466; 1998, Materials Park, OH, USA, ASM International.
8. P. S. Wei, Y. K. Kuo and J. S. Ku: *J. Heat Transfer (Trans. ASME)*, 2000, **122**, 626–631.
9. W. M. Steen: 'Laser material processing'; 1991, New York, Springer-Verlag.
10. W. Duley: 'Laser welding'; 1999, New York, John Wiley and Sons.
11. P. S. Wei and F. K. Chung: *Metall. Mater. Trans. B*, 2000, **31B**, 1387–1403.
12. G. Phanikumar, K. Chattopadhyay and P. Dutta: *Int. J. Numer. Meth. Heat Fluid Flow*, 2001, **11**, (2), 156–171.
13. R. Chakraborty: 'Numerical study of Marangoni convection in two dissimilar liquids separated horizontally', MSc(Engg) thesis, Indian Institute of Science, Bangalore, India, 2001.
14. S. Kumar, G. Phanikumar, P. Dutta and K. Chattopadhyay: *J. Mater. Sci.*, 2002, **37**, (11), 2345–2349.
15. E. A. Brandes: 'Smithells metals reference book', 6th edn, chapter 14; 1983, London, Butterworths.
16. G. Phanikumar, P. Dutta and K. Chattopadhyay: *Metall. Mater. Trans. B*, 2004, **35B**, 339–350.
17. M. Gremaud, M. Carrard and W. Kurz: *Acta Metall. Mater.*, 1991, **39**, 1431–1443.
18. P. S. Mohanty and J. Mazumder: *Metall. Mater. Trans. B*, 1998, **29B**, 1269–1279.
19. G. Pascoe and J. Mackowiak: *J. Inst. Met.*, 1970, **98**, 253–256.
20. S. A. David and J. M. Vitek: *Int. Mater. Rev.*, 1989, **34**, 213–245.
21. F. Hodaj and P. J. Desre: *Acta Mater.*, 1996, **44**, 4485–4490.